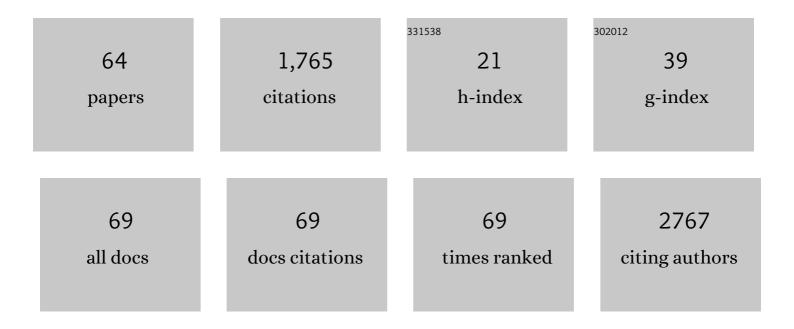
## Harri Merisaari

List of Publications by Year in descending order

Source: https://exaly.com/author-pdf/6470513/publications.pdf Version: 2024-02-01



#	Article	IF	CITATIONS
1	Detection of Prostate Cancer Using Biparametric Prostate <scp>MRI</scp> , Radiomics, and Kallikreins: A Retrospective Multicenter Study of Men With a Clinical Suspicion of Prostate Cancer. Journal of Magnetic Resonance Imaging, 2022, 55, 465-477.	1.9	9
2	Feasibility of FreeSurfer Processing for T1-Weighted Brain Images of 5-Year-Olds: Semiautomated Protocol of FinnBrain Neuroimaging Lab. Frontiers in Neuroscience, 2022, 16, 874062.	1.4	8
3	Association between Incidental Pelvic Inflammation and Aggressive Prostate Cancer. Cancers, 2022, 14, 2734.	1.7	5
4	Subcortical and hippocampal brain segmentation in 5â€yearâ€old children: Validation of FSLâ€FIRST and FreeSurfer against manual segmentation. European Journal of Neuroscience, 2022, 56, 4619-4641.	1.2	7
5	Test-retest repeatability of a deep learning architecture in detecting and segmenting clinically significant prostate cancer on apparent diffusion coefficient (ADC) maps. European Radiology, 2021, 31, 379-391.	2.3	15
6	The impact of edema and fiber crossing on diffusion MRI metrics assessed in an ex vivo nerve phantom: Multiâ€ŧensor model vs. diffusion orientation distribution function. NMR in Biomedicine, 2021, 34, e4414.	1.6	10
7	A variation in the infant oxytocin receptor gene modulates infant hippocampal volumes in association with sex and prenatal maternal anxiety. Psychiatry Research - Neuroimaging, 2021, 307, 111207.	0.9	6
8	Docetaxel chemotherapy response in PC3 prostate cancer mouse model detected by rotating frame relaxations and water diffusion. NMR in Biomedicine, 2021, 34, e4483.	1.6	1
9	Whole Brain Adiabatic T 1rho and Relaxation Along a Fictitious Field Imaging in Healthy Volunteers and Patients With Multiple Sclerosis: Initial Findings. Journal of Magnetic Resonance Imaging, 2021, 54, 866-879.	1.9	1
10	Negative Predictive Value of Biparametric Prostate Magnetic Resonance Imaging in Excluding Significant Prostate Cancer: A Pooled Data Analysis Based on Clinical Data from Four Prospective, Registered Studies. European Urology Focus, 2021, 7, 522-531.	1.6	10
11	Statistical Evaluation of Different Mathematical Models for Diffusion Weighted Imaging of Prostate Cancer Xenografts in Mice. Frontiers in Oncology, 2021, 11, 583921.	1.3	1
12	Computer extracted gland features from H&E predicts prostate cancer recurrence comparably to a genomic companion diagnostic test: a large multi-site study. Npj Precision Oncology, 2021, 5, 35.	2.3	13
13	Comparative analysis of 1152 African-American and European-American men with prostate cancer identifies distinct genomic and immunological differences. Communications Biology, 2021, 4, 670.	2.0	50
14	Infant and Child MRI: A Review of Scanning Procedures. Frontiers in Neuroscience, 2021, 15, 666020.	1.4	38
15	Visual MRI T-category versus VI-RADS evaluation from multiparametric MRI in the detection of muscle-invasion in patients with suspected bladder cancer: single centre registered clinical trial (MIB-trial). Scandinavian Journal of Urology, 2021, 55, 354-360.	0.6	5
16	Whole Brain Adiabatic T 1rho and Relaxation Along a Fictitious Field Imaging in Healthy Volunteers and Patients With Multiple Sclerosis: Initial Findings. Journal of Magnetic Resonance Imaging, 2021, 54, spcone.	1.9	0
17	Signal to noise and b-value analysis for optimal intra-voxel incoherent motion imaging in the brain. PLoS ONE, 2021, 16, e0257545.	1.1	3
18	How to read biparametric MRI in men with a clinical suspicious of prostate cancer: Pictorial review for beginners with public access to imaging, clinical and histopathological database. Acta Radiologica Open, 2021, 10, 205846012110607.	0.3	1

HARRI MERISAARI

#	Article	IF	CITATIONS
19	Repeatability of radiomics and machine learning for DWI: Shortâ€ŧerm repeatability study of 112 patients with prostate cancer. Magnetic Resonance in Medicine, 2020, 83, 2293-2309.	1.9	23
20	Prediction of biochemical recurrence in prostate cancer patients who underwent prostatectomy using routine clinical prostate multiparametric MRI and decipher genomic score. Journal of Magnetic Resonance Imaging, 2020, 51, 1075-1085.	1.9	24
21	Prostate Cancer Risk Stratification in Men With a Clinical Suspicion of Prostate Cancer Using a Unique Biparametric MRI and Expression of 11 Genes in Apparently Benign Tissue: Evaluation Using Machineâ€Learning Techniques. Journal of Magnetic Resonance Imaging, 2020, 51, 1540-1553.	1.9	3
22	Prebiopsy IMPROD Biparametric Magnetic Resonance Imaging Combined with Prostate-Specific Antigen Density in the Diagnosis of Prostate Cancer: An External Validation Study. European Urology Oncology, 2020, 3, 648-656.	2.6	18
23	Qualitative and Quantitative Reporting of a Unique Biparametric MRI: Towards Biparametric MRIâ€Based Nomograms for Prediction of Prostate Biopsy Outcome in Men With a Clinical Suspicion of Prostate Cancer (IMPROD and MULTIâ€IMPROD Trials). Journal of Magnetic Resonance Imaging, 2020, 51, 1556-1567.	1.9	22
24	Sexâ€specific association between infant caudate volumes and a polygenic risk score for major depressive disorder. Journal of Neuroscience Research, 2020, 98, 2529-2540.	1.3	10
25	Partial Support for an Interaction Between a Polygenic Risk Score for Major Depressive Disorder and Prenatal Maternal Depressive Symptoms on Infant Right Amygdalar Volumes. Cerebral Cortex, 2020, 30, 6121-6134.	1.6	21
26	Prediction of prostate cancer aggressiveness using 18F-Fluciclovine (FACBC) PET and multisequence multiparametric MRI. Scientific Reports, 2020, 10, 9407.	1.6	3
27	Newborn amygdalar volumes are associated with maternal prenatal psychological distress in a sex-dependent way. NeuroImage: Clinical, 2020, 28, 102380.	1.4	25
28	Added value of systematic biopsy in men with a clinical suspicion of prostate cancer undergoing biparametric MRI-targeted biopsy: multi-institutional external validation study. World Journal of Urology, 2020, 39, 1879-1887.	1.2	15
29	Newborn white matter microstructure moderates the association between maternal postpartum depressive symptoms and infant negative reactivity. Social Cognitive and Affective Neuroscience, 2020, 15, 649-660.	1.5	15
30	Restingâ€state networks of the neonate brain identified using independent component analysis. Developmental Neurobiology, 2020, 80, 111-125.	1.5	15
31	Association of Cumulative Paternal Early Life Stress With White Matter Maturation in Newborns. JAMA Network Open, 2020, 3, e2024832.	2.8	14
32	MP81-15 TWO-MINUTE PROSTATE MAGNETIC RESONANCE IMAGING PREDICTS GLEASON SCORE: AN ADVANCED MACHINE LEANING OF RAPID T2-WEIGHTED IMAGING. Journal of Urology, 2020, 203, .	0.2	0
33	PD57-05 A DEEP LEARNING NETWORK ALONG WITH PIRADS CAN DISTINGUISH CLINICALLY SIGNIFICANT AND INSIGNIFICANT PROSTATE CANCER ON BI-PARAMETRIC MRI. Journal of Urology, 2020, 203, e1195.	0.2	Ο
34	Radiomics and machine learning of multisequence multiparametric prostate MRI: Towards improved non-invasive prostate cancer characterization. PLoS ONE, 2019, 14, e0217702.	1.1	76
35	A Novel Approach for Manual Segmentation of the Amygdala and Hippocampus in Neonate MRI. Frontiers in Neuroscience, 2019, 13, 1025.	1.4	25
36	Correlation between 18F-1-amino-3-fluorocyclobutane-1-carboxylic acid (18F-fluciclovine) uptake and expression of alanine-serine-cysteine-transporter 2 (ASCT2) and L-type amino acid transporter 1 (LAT1) in primary prostate cancer. EJNMMI Research, 2019, 9, 50.	1.1	14

HARRI MERISAARI

#	Article	IF	CITATIONS
37	T58. Larger Newborn Left Amygdala Volume Predicts Poorer Working Memory in Toddlerhood. Biological Psychiatry, 2019, 85, S151.	0.7	0
38	Validation of IMPROD biparametric MRI in men with clinically suspected prostate cancer: A prospective multi-institutional trial. PLoS Medicine, 2019, 16, e1002813.	3.9	43
39	Test-retest reliability of Diffusion Tensor Imaging metrics in neonates. NeuroImage, 2019, 197, 598-607.	2.1	31
40	IMPROD biparametric MRI in men with a clinical suspicion of prostate cancer (IMPROD Trial): Sensitivity for prostate cancer detection in correlation with wholeâ&mount prostatectomy sections and implications for focal therapy. Journal of Magnetic Resonance Imaging, 2019, 50, 1641-1650.	1.9	16
41	Prenatal exposures and infant brain: Review of magnetic resonance imaging studies and a population description analysis. Human Brain Mapping, 2019, 40, 1987-2000.	1.9	42
42	Associations of age and sex with brain volumes and asymmetry in 2–5-week-old infants. Brain Structure and Function, 2019, 224, 501-513.	1.2	44
43	Sex difference in brain CB1 receptor availability in man. NeuroImage, 2019, 184, 834-842.	2.1	65
44	Neural correlates of gentle skin stroking in early infancy. Developmental Cognitive Neuroscience, 2019, 35, 36-41.	1.9	102
45	Prevalence and Risk Factors of Incidental Findings in Brain MRIs of Healthy Neonates—The FinnBrain Birth Cohort Study. Frontiers in Neurology, 2019, 10, 1347.	1.1	30
46	Prospective evaluation of 18F-FACBC PET/CT and PET/MRI versus multiparametric MRI in intermediate- to high-risk prostate cancer patients (FLUCIPRO trial). European Journal of Nuclear Medicine and Molecular Imaging, 2018, 45, 355-364.	3.3	66
47	11C-acetate PET/MRI in bladder cancer staging and treatment response evaluation to neoadjuvant chemotherapy: a prospective multicenter study (ACEBIB trial). Cancer Imaging, 2018, 18, 25.	1.2	22
48	Fitting methods for intravoxel incoherent motion imaging of prostate cancer on region of interest level: Repeatability and gleason score prediction. Magnetic Resonance in Medicine, 2017, 77, 1249-1264.	1.9	48
49	Novel biparametric MRI and targeted biopsy improves risk stratification in men with a clinical suspicion of prostate cancer (IMPROD Trial). Journal of Magnetic Resonance Imaging, 2017, 46, 1089-1095.	1.9	75
50	Identification of NCAN as a candidate gene for developmental dyslexia. Scientific Reports, 2017, 7, 9294.	1.6	15
51	Patient-specific pharmacokinetic parameter estimation on dynamic contrast-enhanced MRI of prostate: Preliminary evaluation of a novel AIF-free estimation method. Journal of Magnetic Resonance Imaging, 2016, 44, 1405-1414.	1.9	3
52	Relaxation along fictitious field, diffusion-weighted imaging, and T <sub>2</sub> mapping of prostate cancer: Prediction of cancer aggressiveness. Magnetic Resonance in Medicine, 2016, 75, 2130-2140.	1.9	15
53	Diffusion weighted imaging of prostate cancer: Prediction of cancer using texture features from parametric maps of the monoexponential and kurtosis functions. , 2016, , .		6
54	Rotating frame relaxation imaging of prostate cancer: Repeatability, cancer detection, and Gleason score prediction. Magnetic Resonance in Medicine, 2016, 75, 337-344.	1.9	16

HARRI MERISAARI

#	Article	IF	CITATIONS
55	Prospective evaluation of planar bone scintigraphy, SPECT, SPECT/CT, <sup>18</sup> F-NaF PET/CT and whole body 1.5T MRI, including DWI, for the detection of bone metastases in high risk breast and prostate cancer patients: SKELETA clinical trial. Acta Oncológica, 2016, 55, 59-67.	0.8	166
56	Mathematical models for diffusionâ€weighted imaging of prostate cancer using b values up to 2000 s/mm <sup>2</sup> : Correlation with Gleason score and repeatability of region of interest analysis. Magnetic Resonance in Medicine, 2015, 74, 1116-1124.	1.9	53
57	Optimization of <i>b</i> -value distribution for four mathematical models of prostate cancer diffusion-weighted imaging using <i>b</i> values up to 2000 s/mm <sup>2</sup> : Simulation and repeatability study. Magnetic Resonance in Medicine, 2015, 73, 1954-1969.	1.9	52
58	Evaluation of different mathematical models for diffusion-weighted imaging of normal prostate and prostate cancer using high b-values: A repeatability study. Magnetic Resonance in Medicine, 2015, 73, 1988-1998.	1.9	72
59	Prebiopsy multiparametric 3T prostate MRI in patients with elevated PSA, normal digital rectal examination, and no previous biopsy. Journal of Magnetic Resonance Imaging, 2015, 41, 1394-1404.	1.9	47
60	Diffusion-weighted imaging of prostate cancer: effect of b-value distribution on repeatability and cancer characterization. Magnetic Resonance Imaging, 2015, 33, 1212-1218.	1.0	23
61	Optimization of b-value distribution for biexponential diffusion-weighted MR imaging of normal prostate. Journal of Magnetic Resonance Imaging, 2014, 39, 1213-1222.	1.9	37
62	Gaussian mixture model-based segmentation of MR images taken from premature infant brains. Journal of Neuroscience Methods, 2009, 182, 110-122.	1.3	20
63	Effects of intravenous glucose on dopaminergic function in the human brain in vivo. Synapse, 2007, 61, 748-756.	0.6	122
64	Evaluation of partial volume effect correction methods for brain positron emission tomography: Quantification and reproducibility. Journal of Medical Physics, 2007, 32, 108.	0.1	21